Dispersion-compensated wavelength beam combining of quantum-cascade-laser arrays

Anish K. Goyal,[1,*] Melissa Spencer,[1] Oleg Shatrovoy,[1] Benjamin G. Lee,[2,3] Laurent Diehl,[2,4] Christian Pfluegl,[2,4] Antonio Sanchez,[1] and Federico Capasso[2]

[1]*MIT Lincoln Laboratory, 244 Wood Street, Lexington, Massachusetts 02420, USA*
[2]*Harvard University, School of Engineering and Applied Sciences, Cambridge, Massachusetts 02138, USA*
[3] *Currently with the National Renewable Energy Laboratory, 1617 Cole Boulevard, Golden, Colorado 80401, USA*
[4] *Currently with Eos Photonics, 30 Spinelli Place, Cambridge, Massachusetts 02138, USA*
[*]*agoyal@ll.mit.edu*

Abstract: A multiwavelength array of distributed feedback (DFB) quantum cascade lasers (QCLs) that spans λ = 8.28 to 9.62 μm is wavelength beam combined (WBC) using both single-grating and dual-grating designs. WBC with a single grating results in a pointing error of 3-times the beam divergence for a single laser and arises from the nonlinear dispersion of the grating. By adding a second grating to compensate for the nonlinear dispersion, the pointing error is reduced to only 13% of the beam divergence for a single laser. A transceiver based on the dual-grating-WBC QCL was used to measure the transmittance of a polymer sheet placed between itself and a retroreflector over a round-trip distance of 70 meters.

OCIS codes: (140.5965) Semiconductor lasers, quantum cascade; (140.3298) Laser beam combining; (140.3490) Lasers, distributed-feedback; (140.3290) Laser arrays.

References and links

1. F. Capasso, C. Gmachl, D. L. Sivco, and A. Y. Cho, "Quantum cascade lasers," Phys. Today **55**(5), 34–40 (2002).
2. R. Curl, F. Capasso, C. Gmachl, A. A. Kosterev, B. McManus, R. Lewicki, M. Pusharsky, G. Wysocki, and F. K. Tittel, "Quantum cascade lasers in chemical physics," Chem. Phys. Lett. **487**(1-3), 1–18 (2010).
3. A. Kosterev and F. Tittel, "Chemical sensors based on quantum cascade lasers," IEEE J. Quantum Electron. **38**(6), 582–591 (2002).
4. R. Maulini, A. Mohan, M. Giovannini, J. Faist, and E. Gini, "External cavity quantum-cascade lasers tunable from 8.2 to 10.4 μm using a gain element with a heterogeneous cascade," Appl. Phys. Lett. **88**(20), 201113 (2006).
5. A. Hugi, R. Terazzi, Y. Bonetti, A. Wittmann, M. Fischer, M. Beck, J. Faist, and E. Gini, "External cavity quantum cascade laser tunable from 7.6 to 11.4 μm," Appl. Phys. Lett. **95**(6), 061103 (2009).
6. Daylight Solutions, Inc., *www.daylightsolutions.com*.
7. B. G. Lee, M. A. Belkin, R. Audet, J. MacArthur, L. Diehl, C. Pflügl, F. Capasso, D. Oakley, D. Chapman, A. Napoleone, D. Bour, S. Corzine, G. Hofler, and J. Faist, "Widely tunable single-mode quantum cascade laser source for mid-infrared spectroscopy," Appl. Phys. Lett. **91**(23), 231101 (2007).
8. B. G. Lee, H. A. Zhang, C. Pflügl, L. Diehl, M. A. Belkin, M. Fischer, A. Wittmann, J. Faist, and F. Capasso, "Broadband distributed-feedback quantum cascade laser array operating from 8.0 to 9.8 μm," IEEE Photon. Technol. Lett. **21**(13), 914–916 (2009).
9. B. G. Lee, M. A. Belkin, C. Pflügl, L. Diehl, H. A. Zhang, R. M. Audet, J. MacArthur, D. P. Bour, S. W. Corzine, G. E. Höfler, and F. Capasso, "DFB quantum cascade laser arrays," IEEE J. Quantum Electron. **45**(5), 554–565 (2009).
10. T. Y. Fan, "Laser beam combining for high-power, high-radiance sources," IEEE J. Sel. Top. Quantum Electron. **11**(3), 567–577 (2005).
11. B. G. Lee, J. Kansky, A. K. Goyal, C. Pflügl, L. Diehl, M. A. Belkin, A. Sanchez, and F. A. Capasso, "Beam combining of quantum cascade laser arrays," Opt. Express **17**(18), 16216–16224 (2009).
12. S. Hugger, R. Aidam, W. Bronner, F. Fuchs, R. Lösch, Q. Yang, J. Wagner, E. Romasew, M. Raab, H. D. Tholl, B. Höfer, and A. L. Matthes, "Power scaling of quantum cascade lasers via multiemitter beam combining," Opt. Eng. **49**(11), 111111 (2010).
13. G. M. Russwurm and J. W. Childers, "Open-path Fourier Transform Infrared Spectroscopy," in *Handbook of Vibrational Spectroscopy*, J. M. Chalmers and P. R. Griffiths, ed. (Wiley, 2002).

#154488 - $15.00 USD Received 12 Sep 2011; revised 5 Nov 2011; accepted 7 Nov 2011; published 14 Dec 2011

1. Introduction

Quantum cascade lasers (QCLs) are electrically driven semiconductor lasers that can operate in spectral bands ranging from the mid-infrared (MIR) to the terahertz [1]. Of great interest is the so-called MIR "molecular fingerprint" region ($\lambda \approx 3$–14 μm) in which molecules may be identified based on strong and unique absorption bands related to their vibrational-rotational modes [2]. For the detection of relatively simple molecules in the gaseous state that have very narrow absorption bands, spectral tunability may only be required over a narrow frequency range of <3 cm^{-1} in which case a thermally tuned distributed feedback (DFB) QCL may be used [3]. But when broader tunability is required, the QCL is typically incorporated into a frequency-selective external-cavity [4]. Recently, tuning over 432 cm^{-1} (from $\lambda = 7.6$–11.4 μm) has been reported from an external-cavity QCL (EC-QCL) [5]. Since tuning of EC-QCLs occurs through mechanical means, it takes on the order of 1 second to scan the full spectral range [6]. For many applications, it is desirable to tune much faster. An alternative to EC-QCLs is a multiwavelength array of QCLs in which the emission wavelength is determined simply by driving the appropriate laser in the array [7]. QCL arrays enable extremely fast wavelength tuning with no moving parts.

We previously demonstrated spectroscopy using a multiwavelength array of distributed feedback (DFB) QCLs [7]. The emission frequency of each laser is determined by the period of the DFB grating embedded within the semiconductor waveguide. Arrays were designed such that adjacent lasers are spaced equally in frequency by either ~3 cm^{-1} or ~10 cm^{-1} [8, 9]. Although temperature tuning could be used to continuously access all wavelengths that are spanned by the array, for many chemicals of interest the absorption features are relatively broad (10's of cm^{-1}) and require only modest spectral resolution. In such cases, continuous tunability is not required. In order to interrogate a distant target using these QCL arrays, it is necessary to spatially overlap all of the laser beams. In our prior work, we used a standard open-loop wavelength-beam-combining (WBC) optical system [10] that incorporates a single diffraction grating to overlap the laser beams [11]. It was determined, however, that the beams could not be perfectly overlapped because of nonlinearity in the dispersion of the diffraction grating. Nevertheless, we were able to demonstrate remote spectroscopy of isopropyl alcohol at a range of 3 meters which was limited by the pointing error of elements in the array. In the present work, we experimentally demonstrate that the nonlinear components of the dispersion from a diffraction grating in the WBC geometry can be compensated by using a second diffraction grating. This enables the pointing error to be a small fraction of the beam divergence of each laser element. This source was used in a proof-of-principle demonstration of remote spectroscopy over a round-trip path of 70 meters. The range was not limited by the degree of spatial overlap of the laser beams but by the laser power and size of the optics that were used. With appropriate optics and higher power lasers, line-of-sight spectroscopy could be achieved over many kilometers.

2. Experimental

2.1 Laser array

The DFB-QCL array used for this work is designed for broadband gain and includes up to 32 DFB lasers that are individually addressable [8]. The 15-μm-wide laser ridges have a pitch of 75 μm. The inset of Fig. 1 shows a laser chip which is subsequently bonded epi-side up to a copper heat-sink and the individual lasers are wire-bonded to separate traces on a printed circuit board. The lasers are driven under pulsed conditions (typically 50 ns, 10 kHz, room temperature) by a custom current driver that is computer controlled via a serial interface to allow firing of the lasers in an arbitrary order.

The array used for the present experiments contains 19 operating lasers, but usually only 15 of the more powerful lasers were used for the WBC results that are presented. The maximum peak output power for these lasers was as high as 130 mW. For reasons described in Ref. 9, the maximum peak power for lasers in the array varies by about an order-of-

#154488 - $15.00 USD Received 12 Sep 2011; revised 5 Nov 2011; accepted 7 Nov 2011; published 14 Dec 2011

magnitude such that the weakest laser has a maximum peak power of 20 mW. The DFB grating period was designed such that the laser frequency varies linearly with position along the array. Figure 1 plots the laser frequency versus laser number. The laser frequencies span ν = 1208 to 1039 cm^{-1} (λ = 8.28 to 9.62 μm) with a spacing between adjacent lasers of about 9.4 cm^{-1}. The small deviation from linearity is such that the frequency of the center laser is offset by ~2 cm^{-1} from a linear interpolation that connects the outermost lasers.

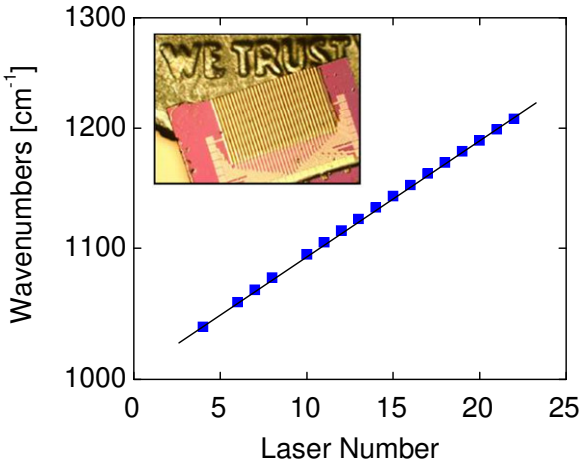

Fig. 1. Laser frequency versus laser number for the multiwavelength DFB QCL array used in this work. The inset is a photograph of an array.

2.2 WBC with a single grating

WBC was first performed using a single diffraction grating. As schematically depicted in Fig. 2, an anti-reflection (AR) coated ZnSe lens with f_T = 12.7 mm (D = 12.7 mm) was placed one focal length away from the array. The diffraction grating (50 g/mm, 12-μm-blaze) was placed one focal length away from the lens. The angle-of-incidence (AOI), relative to the grating normal, is nominally 50.9° for the center laser. Experimentally, this angle was adjusted to overlap the first-order diffracted beams from lasers #4 and #22 in the far-field.

The near-field was measured a few centimeters from the grating and is well approximated by an elliptical truncated Gaussian with dimensions of 16 mm × 11 mm in the WBC and non-WBC dimensions, respectively, as measured at the full-width-at-1/e^2 (FW1/e^2) intensity points. The beam emitted from the QCL is highly divergent and overfills the lens. As a result, the beam in the non-WBC (vertical) dimension is approximately equal to the lens diameter. In the WBC (horizontal) dimension, the beam expands to 16 mm due to the 1.5-times geometric magnification of the grating. The far-field shown in the inset of Fig. 2 was measured at the focus of a spherical mirror (f = 1.44 m). The far-field is an elliptical Airy function with a divergence of 1.2 mrad × 1.8 mrad FW1/e^2. The beam quality is calculated using a times-diffraction-limited (TDL) metric for Gaussian beams given by $\pi W\theta/4\lambda$ where W is the FW1/e^2 near-field size, θ is the FW1/e^2 far-field divergence, and λ is the wavelength. Using this definition, the beam quality is ~1.7 TDL in both dimensions. The non-ideal beam quality is presumably due to aberrations from the transform lens.

The beam pointing of each laser was determined from the centroid of the far-field intensity profile. Figure 2 plots the beam pointing in the WBC dimension as a function of laser number when the end lasers of the array are overlapped. The pointing error is approximately quadratic versus laser number with a peak-to-peak pointing error of 3.6 mrad. This pointing error was also observed in our previous work [11] and is due to the nonlinear

#154488 - $15.00 USD Received 12 Sep 2011; revised 5 Nov 2011; accepted 7 Nov 2011; published 14 Dec 2011

dispersion of the grating. The solid line in the plot of Fig. 2 is a theoretical calculation using the following equation which is based on the standard grating equation

$$\alpha_i = \sin^{-1}\left\{\sin\left[\beta_o - \tan^{-1}\left(\frac{\Delta x}{f_T}\right)\right] - \frac{\lambda_i}{d}\right\} \quad (1)$$

where f_T is the focal length of the transform lens, d is the grating period, and β_o is the angle of incidence for the on-axis laser relative to the grating normal. The subscript i refers to the laser number for the wavelength λ_i, distance from the lens axis Δx_i, and the diffracted angle α_i. The correspondence between measurement and theory is excellent. The *relative* pointing error, which we define as the peak-to-peak pointing error divided by the FW1/e^2 beam divergence, is 3. Because the pointing error is large relative to the beam divergence of a single laser, this source is not suitable for remote spectroscopy over long distances because all lasers in the array will not interrogate the same target or be captured by a common detector.

The relative pointing error cannot be significantly reduced by simply choosing a different combination of lens and diffraction grating. In fact, the minimum relative pointing error is calculated to be 2 when using the existing QCL array and a single grating for WBC. One method to reduce the relative pointing error to insignificant levels is to adjust the laser frequency versus position during fabrication to precisely match the grating dispersion. This can be achieved, for instance, by maintaining a constant laser pitch and varying the frequency spacing between adjacent lasers. Another solution, which was implemented as described below with the existing QCL array, is to add a second grating to linearize the grating dispersion. As described in the next section, it is found that the nonlinear components of the dispersion can be reduced to negligible levels by adding a second grating.

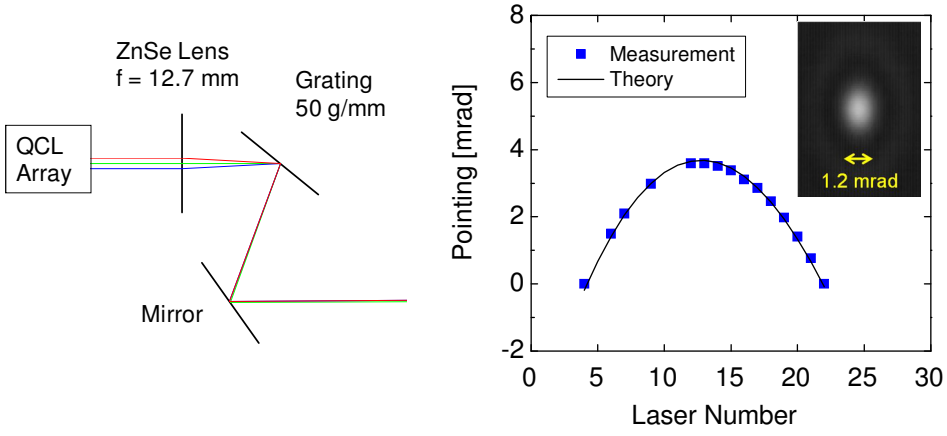

Fig. 2. Ray-trace diagram of the single-grating WBC configuration (left). Pointing error versus laser number for the single-grating WBC configuration (right). The peak-to-peak pointing error is 3.6 mrad. The inset shows an image of the far-field of a single laser which has a beam divergence of 1.2 mrad FW1/e^2 in the WBC dimension.

2.3 WBC using a second grating for dispersion compensation

The dual-grating design is schematically depicted in Fig. 3. The first grating imposes a dispersion that is greater than needed to spatially overlap the lasers at opposite ends of the array. The second grating then reduces the average dispersion to the desired value while substantially canceling the nonlinear components. Figure 3 also plots the calculated pointing error as a function of the grating groove density for the two gratings given f_T = 2.5 cm. For each grating combination, the grating angles that minimized the pointing error of the central laser relative to the lasers at opposite ends of the array are found numerically. The pointing

#154488 - $15.00 USD Received 12 Sep 2011; revised 5 Nov 2011; accepted 7 Nov 2011; published 14 Dec 2011

error determined in this way is plotted on a $\log_{10}$ scale. As can be seen, there is a well-defined band over which dispersion compensation is effective in yielding pointing errors of <1 μrad (or relative pointing errors of <<1%). One finds that the first grating should have a higher groove density than the second grating. This is consistent with the idea of using the second grating to partially compensate for the dispersion from the first grating. In order to choose a specific design within the range of possible solutions, several additional factors were taken into consideration. First, the design must be physically realizable in that the ray paths are not obstructed by optical components. Also, the grating magnification should not be too large. A large grating magnification will increase both the size of the optics as well as the ellipticity of the output beam. The selected design uses grating groove densities of 100 g/mm and 50 g/mm with corresponding AOI = 55.2° and 49.3° for the first and second gratings, respectively. Assuming that the laser frequencies vary exactly linearly with position, the calculated pointing error is <0.2 μrad and the overall grating magnification is 2.5.

Figure 3 depicts the ray-tracing diagram corresponding to this design. The rays from all QCLs start by pointing in the same direction. The beams then converge at a distance of one focal length from the transform lens. For single-grating WBC, the grating would be located at this position. In contrast, for dual-grating WBC the grating is placed beyond this position at a location that is arbitrary to some extent. For the experiments results described below, the distance between the lens and first grating is nominally 7.5 cm. After being diffracted from the first grating, the beams converge at a distance of 4.5 cm where the second grating is placed. It is calculated that the beams do not converge perfectly at the second grating but are offset in the near-field by ~25 μm. This offset is negligible compared to the 11.7-mm beam size. The dual-grating design provides a great deal of flexibility in placement of the gratings. This is useful for avoiding optical obscurations and mechanical interferences.

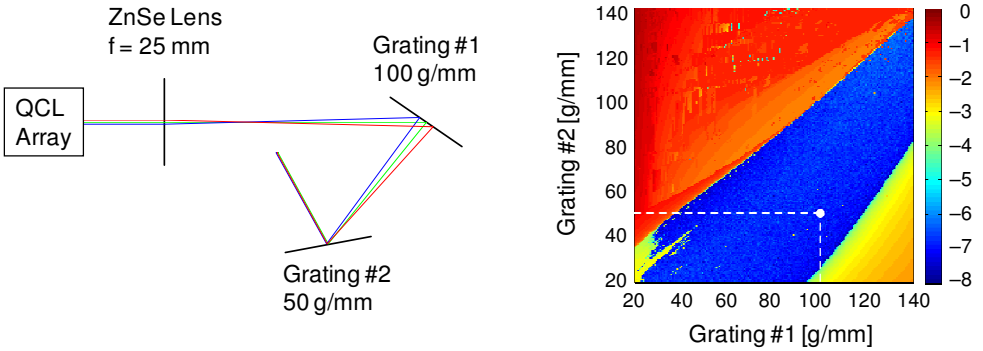

Fig. 3. Ray-trace diagram of the dual-grating WBC configuration that was implemented in this work (left). Calculated peak-to-peak pointing error versus the groove densities for the two gratings in a dual-grating WBC configuration (right). The pointing error is normalized by 1 radian and plotted on a $\log_{10}$ scale for a transform lens with focal length of f_T = 2.5 cm. The design point is indicated.

For the dual-grating WBC experiments, a microlens array was integrated with the QCL array. The microlens array has the effect of increasing the far-field divergence from the system by reducing the near-field beam size at the gratings. As compared to a system without microlenses, microlenses will reduce the *relative* pointing error while the *absolute* pointing error remains unchanged. The germanium microlens array is AR coated on both surfaces. Each lens has a spherical surface-figure corresponding to f = 75 μm to collimate the beam in both the slow and fast axes. The lens aperture is rectangular with a pitch of 75 μm in the WBC dimension to match the QCL array and 150 μm in the orthogonal dimension to capture a larger fraction of the rapidly diverging beam from the QCL. Based on the measured profiles of the laser beams after collimation by the microlens (which are well approximated by Gaussians), one infers a footprint of the laser beams at the microlens of 60 μm × 110 μm FW1/e^2. The microlens array was aligned to the QCL array such that the beams are collimated

#154488 - $15.00 USD Received 12 Sep 2011; revised 5 Nov 2011; accepted 7 Nov 2011; published 14 Dec 2011

and pointing in the same direction, and then permanently attached to the laser submount using UV-curing epoxy. Because of the increased numerical aperture of the microlens as compared to the collection lens ($f = D$ = 12. 7 mm) used in the single-grating experiment, the collection efficiency was measured to increase by the factor 1.75.

The microlensed QCL array was incorporated into the dual-grating WBC optical system and the beam properties were characterized using a microbolometer focal-plane-array. The laser near-fields were measured 15 cm from the second grating. For laser #11, the near-field beam size of 11.7 mm x 2.7 mm FW1/e^2 corresponds to an ellipticity of 4.3. This is close to an ellipticity of 4.5 calculated as the product of the ellipticity of the starting beam and the grating magnification. Figure 4(a) plots the beam position in the WBC dimension versus laser number. The length of the bars represents the FW1/e^2 beam sizes and the points indicate the centroids. The peak-to-peak positional error in the WBC dimension is 0.6 mm or only 5% of the 11.7-mm beam size. The beam size is seen to decrease by ~25% with increasing laser number. This is due to the fact that the AOI, and therefore the grating magnification, varies along the array. In the non-WBC dimension, the positional error is 0.35 mm or 13% of the 2.7-mm beam size.

The laser far-fields are measured at the focal plane of a spherical mirror (f = 1.44 m). The far-field divergence for laser #11 is 1.5 mrad × 5.8 mrad FW1/e^2. This corresponds to a beam quality of 1.5 and 1.4 TDL in the WBC and non-WBC dimensions, respectively. Figure 4(b) plots the beam pointing in the WBC dimension. The length of the bars represents the FW1/e^2 beam divergences and the points indicate the pointing error. In the WBC dimension, the peak-to-peak pointing error is 0.2 mrad which is only 13% of the 1.5-mrad beam divergence. This result demonstrates that dispersion compensation using dual-grating WBC has been effective in reducing the pointing error by a factor of 20 as compared to single-grating WBC. The pointing error, however, is larger than the minimum theoretical value. We attribute a portion of this discrepancy to the fact that the frequency spacing of the lasers is not perfectly linear with position. The nonlinear frequency spacing of the laser array accounts for a relative pointing error of ~10%. The balance of the pointing error can be attributed to imprecision in fabrication of the microlens and QCL arrays as well as to beam steering in the QCLs. These results clearly demonstrate that the dual-grating compensation approach significantly reduces the pointing error.

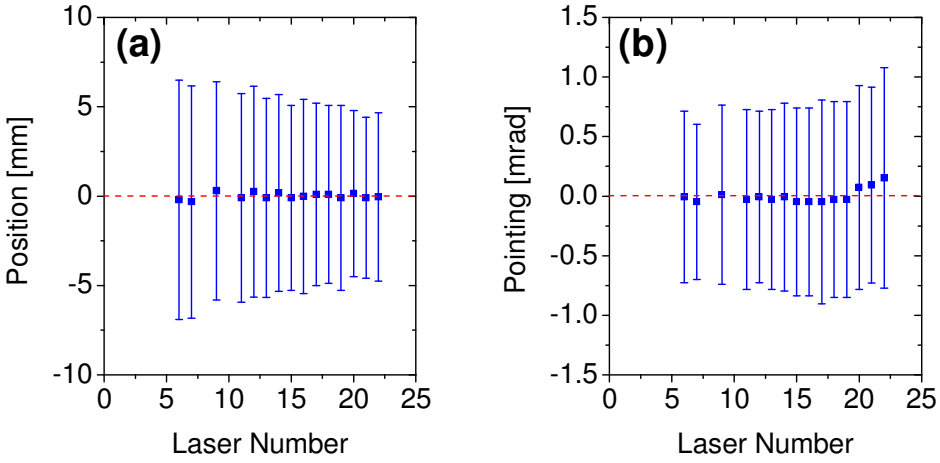

Fig. 4. Measured (a) near-field beam position and (b) far-field beam pointing versus laser number for the dual-grating WBC configuration. The length of the bars represents the FW1/e^2 dimensions and the points represent the centroids.

One drawback of the dual-grating approach is that the WBC efficiency is degraded because of diffraction losses from the additional grating. The WBC efficiency is measured to be ~30% and is calculated as the ratio of laser power after the second grating to the power

#154488 - $15.00 USD Received 12 Sep 2011; revised 5 Nov 2011; accepted 7 Nov 2011; published 14 Dec 2011

after the microlens. This is consistent with the ~50% diffraction efficiency of each grating. The WBC efficiency can be increased somewhat by using gratings with higher diffraction efficiency (e.g., through optimization of the blaze angle). Additionally, since gratings generally have higher diffraction efficiency when operated with the electric-field perpendicular to the grating grooves, a quarter-wave plate can be used to rotate the polarization of the QCL emission [12]. In this case, the diffraction efficiency for commercially available gratings can be in the range of 95% and the WBC efficiency for the dual-grating geometry can be expected to approach 90%. These approaches should be implemented to maximize the efficiency of a system, but such optimization was beyond the scope of the current work.

2.4 Remote spectroscopy demonstration

The WBC QCL-array was incorporated into a transceiver to demonstrate line-of-sight spectroscopy between the transceiver and a distant retroreflector. The output from the WBC QCL-array was circularized using a pair of cylindrical lenses to a diameter of ~1 cm. As schematically depicted in the inset of Fig. 5, this beam was collimated and directed through a 50/50 beam-splitter towards a 6.25-cm-diameter hollow-gold retroreflector placed at a distance of 35 m from the transceiver. The reflected light was captured through a 2-cm-diameter collection aperture and focused onto a fast HgCdTe detector (Vigo PCE-3TE-12 1x1). Because of the limited dynamic range of the receive electronics, the drive current was adjusted on a laser by laser basis to result in a roughly constant transmit power versus wavelength. This power was set by the weakest laser in the array. As a result, taking into account the beam-combining efficiency and throughput of the transmitter optics, the transmit power was about 3 mW (50 ns, 10 kHz). With nothing placed in the beam path, the return signal was measured using an oscilloscope that averaged 8 pulses at each wavelength. Under these conditions, the signal-to-noise ratio of the return signal was ~100. A polymer sheet of unknown composition, but having spectral features in this wavelength band, was then placed in the beam path. The ratio of the return signals with and without the polymer sheet was taken to be its double-pass transmittance. Figure 5 plots the transmittance measured in this way as data points. For comparison, the solid line is the double-pass transmittance measured using a laboratory Fourier-transform infrared (FTIR) spectrometer. The correspondence between measurements is very good. The small discrepancies are attributed to the non-uniform thickness and composition of the polymer film that was used and not to the transceiver system. The measurement time for each wavelength was ~0.3 sec. With optimized electronics, the measurement time per wavelength could be reduced to the order of 100 nsec. The QCL-based source has a spatial brightness which is many orders-of-magnitude greater than a blackbody source [13] and enables open-path spectroscopy over much longer distances. For the measurements described here, the path length was not limited by the degree of spatial overlap of the laser beams, but by the size of the optics that were used. With appropriate optics and higher power lasers, line-of-light spectroscopy can be achieved over many kilometers. In fact, if the optics could be arbitrarily large, the path length would be limited only by atmospheric effects such as absorption and scintillation.

#154488 - $15.00 USD Received 12 Sep 2011; revised 5 Nov 2011; accepted 7 Nov 2011; published 14 Dec 2011

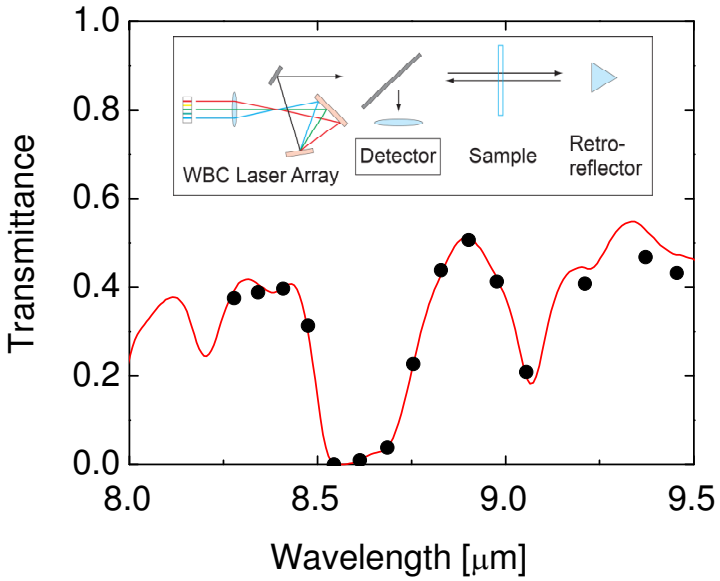

Fig. 5. Double-pass transmittance of a polymer sheet measured using the QCL-based transceiver and a retroreflector at a round-trip path of 70 meters are shown as circles. The inset shows the experimental configuration. The solid line is the reference spectrum taken using a laboratory FTIR spectrometer.

3. Summary

In summary, we demonstrate dual-grating WBC of a DFB-QCL array that achieves low pointing error by compensating for the nonlinear dispersion of a single grating by adding a second grating. A 15-element DFB-QCL array was beam combined using both single and dual-grating approaches. With a single grating, the relative pointing error of 3 (measured with respect to the divergence of a single laser) was due to the nonlinear dispersion of the diffraction grating. By using a second grating to substantially cancel the nonlinear portion of the grating dispersion, the relative pointing error was reduced to 13%. Since the pointing error is much less than the beam divergence of a single laser, this source can be used for spectroscopy over long ranges. As a proof-of-principle spectroscopy demonstration, the dual-grating-WBC QCL-array was incorporated into a transceiver. The transmission spectrum of a polymer sheet was measured when placed between the transceiver and a retroreflector (round trip of 70 meters). The double-pass transmittance measured in this way is in good agreement with measurements made using a laboratory FTIR spectrometer.

Acknowledgments

The Lincoln Laboratory portion of this work was sponsored by the Department of the Air Force under Air Force contract number FA8721-05-C-0002. Opinions, interpretations, conclusions, and recommendations are those of the authors and are not necessarily endorsed by the United States government.

#154488 - $15.00 USD Received 12 Sep 2011; revised 5 Nov 2011; accepted 7 Nov 2011; published 14 Dec 2011